Combined effect of Ni and nano-Y_2O_3 addition on microstructure, mechanical and high temperature response of W-Mo alloy.

Anshuman Patra*, Swapan Kumar Karak
Department of Metallurgical and Materials Engineering, National Institute of Technology, Rourkela, Rourkela - 769008, Odisha, India

*** Presenting author. Email: patraa@nitrkl.ac.in**

Abstract

The present research work deals with the synthesis of nanostructured tungsten (W) based alloys with the nominal compositions of $W_{70}Mo_{30}$ and 1.0 wt. % nano-Y_2O_3 dispersed $W_{79}Ni_{10}Mo_{10}$ (in wt. %) by mechanical alloying followed by compaction at 1GPa pressure for 5 mins and conventional sintering at 1500°C for 2 h in Ar atmosphere. The microstructure and evolution of phases during milling and consolidated products are investigated by X-ray diffraction (XRD) and scanning electron microscopy (SEM) and transmission electron microscopy (TEM). Minimum crystallite size of 29.4 nm and maximum lattice strain and dislocation density of 0.51% and 18.93 ($10^{16}/m^2$) respectively is achieved in 1.0 wt. % nano-Y_2O_3 dispersed $W_{79}Ni_{10}Mo_{10}$ alloy at 20 h of milling. $W_{79}Ni_{10}Mo_{10}$ alloy with 1.0 wt. % nano-Y_2O_3 dispersed alloy shows maximum sintered density, hardness and strength of 95.2%, 9.12 GPa and 1.51 GPa respectively as well as maximum wear and oxidation resistance (at 1000°C) resistance as compared to that of $W_{70}Mo_{30}$.

Keywords: W based alloy, Mechanical alloying, sintering, density, hardness, strength

1. Introduction

Tungsten is used in electrical, electronic, nuclear reactor and space vehicle applications owing to high melting point (3410°C), excellent mechanical strength at elevated temperature, highest density (19.3 g/ml), hardness of 9.8 GPa, high tensile elastic modulus (411 GPa at 20°C) [1,2]. Ultra-fine and uniform dispersion of oxide particles at the grain boundary of tungsten matrix inhibit recrystallization and grain growth for high temperature applications. Dispersed oxides improve high temperature strength and creep resistance by the grain boundary pinning and impeding the grain boundary sliding at high temperature. However poor fabricability, high ductile brittle transition temperature and higher sintering temperature (in excess of 2700°C) limit the use of tungsten from wide spectrum of application [2]. Recent report shows that the sintering temperature of W based alloy could be lowered by fabrication of nanostructured material prior to sintering [3]. Mechanical alloying is a potential candidate for synthesis of nanostructured amorphous or crystalline material [4,5]. Nanostructured material exhibit high strength and hardness as compared to bulk material due to higher degree of microstructural refinement [6].

2. Material and Method

Nanostructured tungsten (W) based alloys with the nominal compositions of $W_{70}Mo_{30}$ and 1.0 wt. % nano-Y_2O_3 dispersed $W_{79}Ni_{10}Mo_{10}$ was subjected to mechanical alloying in a high energy ball mill for 20 h at 300 r.p.m using chrome steel as grinding media and toluene as process control agent. The milled powders at different time of milling were characterized by XRD, SEM, and TEM. The crystallite size, lattice strain of the milled powder was measured by Williamson and Hall method [7]. The dislocation density of the milled powders has been evaluated as below:

$$\rho_d = 2\sqrt{3}\frac{(\varepsilon^2)^{1/2}}{D \times b} \qquad (1)$$

Where, b is the burgers vector of dislocations, b = (a√3)/2 for the bcc structure, a= cell parameter = lattice parameter, D = crystallite size, ε = lattice strain [8-10]. The 20 h milled powders were compacted into pellets by using 1 GPa pressure for 5 mins. The compacted pellets were sintered in Ar atmosphere at 1500°C for 2 h. The sintered density of the alloys was evaluated by Archimedes principle [11, 12]. Micohardness tester and ball on plate wear tester was employed to measure the hardness and wear depth of the sintered alloy. Compression test was carried out to

evaluate the compressive strength of the sintered alloy. Oxidation in air at 1000°C for was conducted for 6 h to investigate the high temperature response of the sintered alloy.

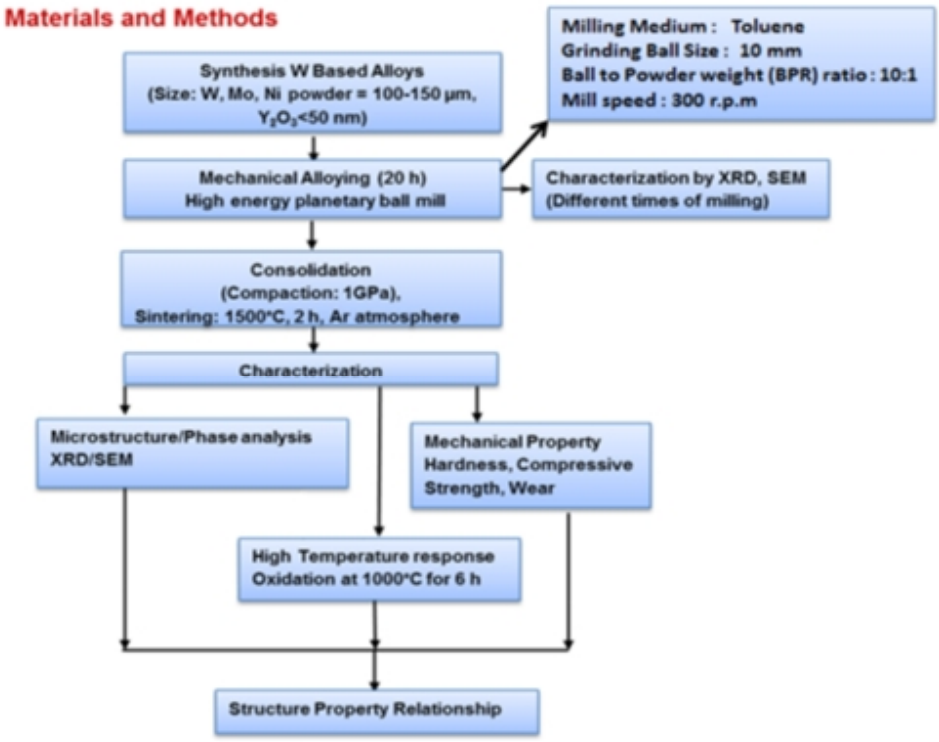

Fig. 1. Process Flow chart

Result and Discussion:

XRD pattern of the milled powder shows reduction in the intensity and broadening of peak (Fig. 2) resulted in reduction in crystallite size (Fig. 3(a)). Same trend was also reported in recent literature [13, 14]. The lattice strain (Fig. 3(b)) and dislocation density (Fig. 4(a)) increases with increase in milling time due to extensive deformation during milling. 1.0 wt. % nano-Y_2O_3 dispersed $W_{79}Ni_{10}Mo_{10}$ alloy shows lower crystallite size and higher lattice strain and dislocation density as compared to $W_{70}Mo_{30}$ alloy. This is attributed to higher energy associated with nano-Y_2O_3. Recent report also suggests same behavior by addition of nano oxides in micro sized particle [15]. Fig. 4(b) illustrates that lattice parameter of W in all the alloys increases upto 10 h of milling due to negative hydrostatic pressure exerted by nano-crystallites [16] and decreases beyond 10 h of milling due to formation of solid solution. SEM micrographs (Fig. 5 and Fig. 6)

display the continuous refinement of the microstructure for both the alloys. Fig. 7 represent the TEM image of 20 h milled $W_{79}Ni_{10}Mo_{10}(Y_2O_3)_1$. Presence of Y_2O_3 is evident after indexing of the SAD pattern (Fig. 7(b)). Fig. 8 shows the XRD pattern of the sintered alloys. Formation of MoNi intermetallic is evident in sintered 1.0 wt. % nano-Y_2O_3 dispersed $W_{79}Ni_{10}Mo_{10}$ alloy as evident from XRD pattern (Fig. 8) and SEM micrograph (Fig. 9(b)) supported by energy dispersive spectroscopy (EDS) pattern (Fig. 9 (d)). No intermetallic is evident from XRD or SEM micrograph of sintered $W_{70}Mo_{30}$ alloy. Fig. 10 (a) reveals the presence of dispersed Y_2O_3 at the grain boundary. The dispersed oxide pin the grain boundary and interact with the dislocation (Fig. 10(b)) to enhance the strength [17]. Fig. 11 shows that sinterability of both the alloys increases with increase in pressure. This is attributed to greater extent of pore reduction at higher pressure which enhances the sintering kinetics. It is evident from Fig. 12 (a) and Fig. 12 (b) that $W_{79}Ni_{10}Mo_{10}(Y_2O_3)_1$ alloy exhibit higher hardness and strength as compared to $W_{70}Mo_{30}$ alloy due to presence of hard MoNi intermetallic and dislocation Y_2O_3 interaction. The improvement of strength and hardness has also reported by Kemp *et al.* [18]. Fig. 13 and Fig. 14 display the fracture surface of the compression tested sample. No severe fracture in $W_{79}Ni_{10}Mo_{10}(Y_2O_3)_1$ alloys is apparent from Fig. 13 (b) and Fig. 14 (b) as compared to $W_{70}Mo_{30}$ alloy. Fig. 15 illustrates that sintered $W_{79}Ni_{10}Mo_{10}(Y_2O_3)_1$ alloy shows lower wear depth as compared to $W_{70}Mo_{30}$ alloy due to higher hardness and strength. It is evident from Fig. 16 (a) that $W_{79}Ni_{10}Mo_{10}(Y_2O_3)_1$ alloy is more resistant to oxidation as compared to $W_{70}Mo_{30}$ alloy due to presence to impervious $NiWO_4$ oxide (Fig. 16(b)) [19]. The presence of $NiWO_4$ oxide scale is also revealed by SEM (Fig 17 (a)) and EDS (Fig 17 (b)) analysis.

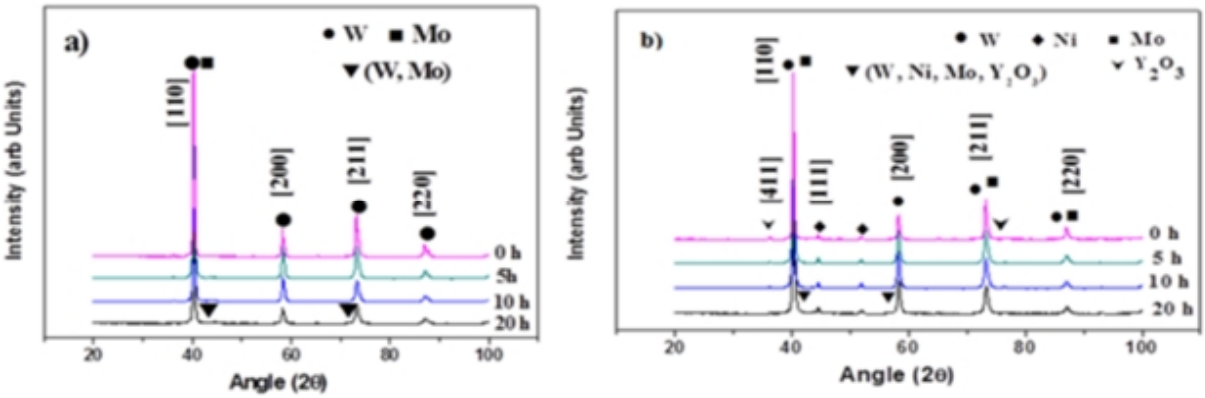

Fig. 2. XRD pattern of powder milled for different times (0, 5, 10, 20 h) a) $W_{70}Mo_{30}$ b) $W_{79}Ni_{10}Mo_{10}(Y_2O_3)_1$

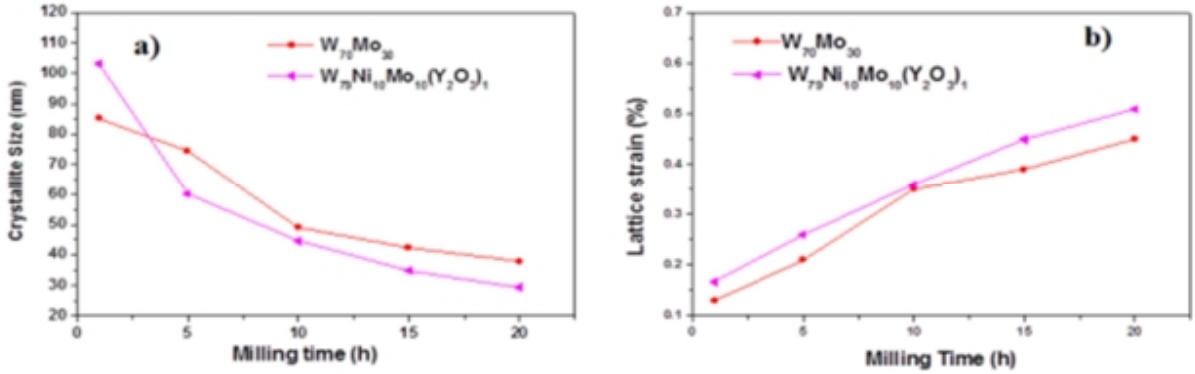

Fig. 3. Variation of a) Crystallite size and b) lattice strain with milling time of alloy $W_{70}Mo_{30}$ and $W_{79}Ni_{10}Mo_{10}(Y_2O_3)_1$.

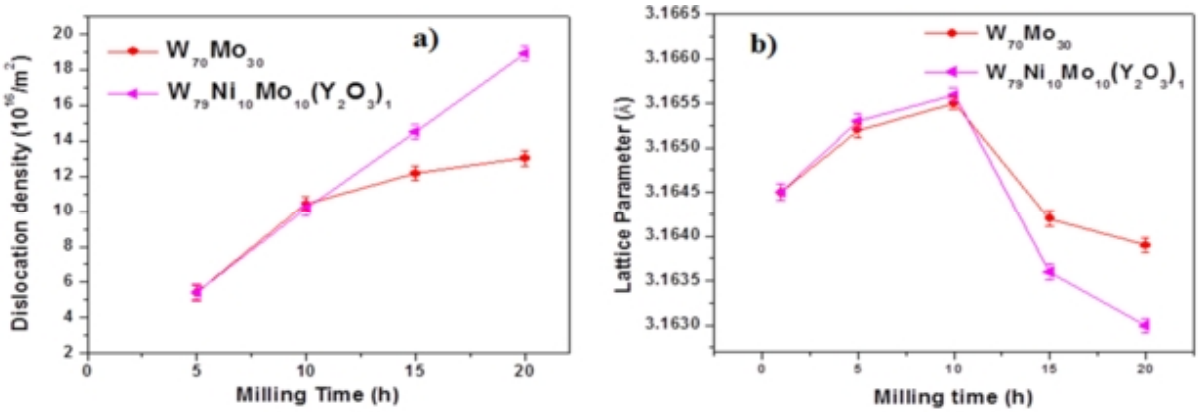

Fig. 4. Variation of a) dislocation density b) lattice parameter with milling time of alloy $W_{70}Mo_{30}$ and $W_{79}Ni_{10}Mo_{10}(Y_2O_3)_1$.

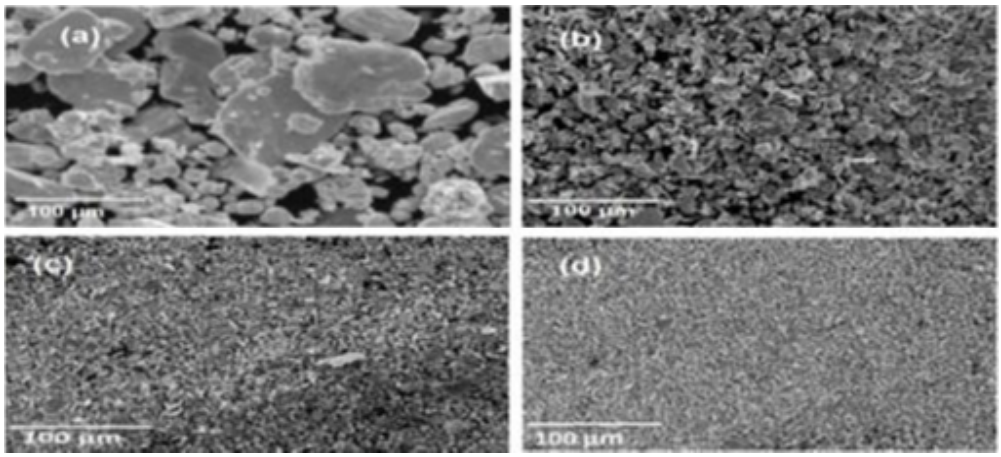

Fig. 5. SEM micrograph of powder morphology of alloy $W_{70}Mo_{30}$ after different milling times: (a) 0 h, (b) 5 h, (c) 10 h, and (d) 20 h.

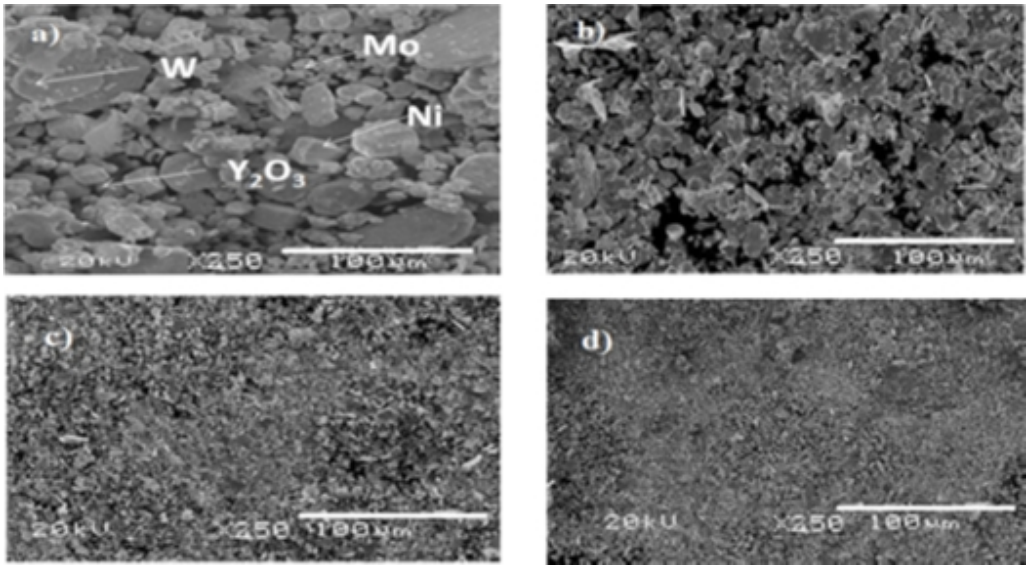

Fig. 6. SEM micrograph of powder morphology of alloy $W_{79}Ni_{10}Mo_{10}(Y_2O_3)_1$ after different milling times: (a) 0 h, (b) 5 h, (c) 10 h, and (d) 20 h.

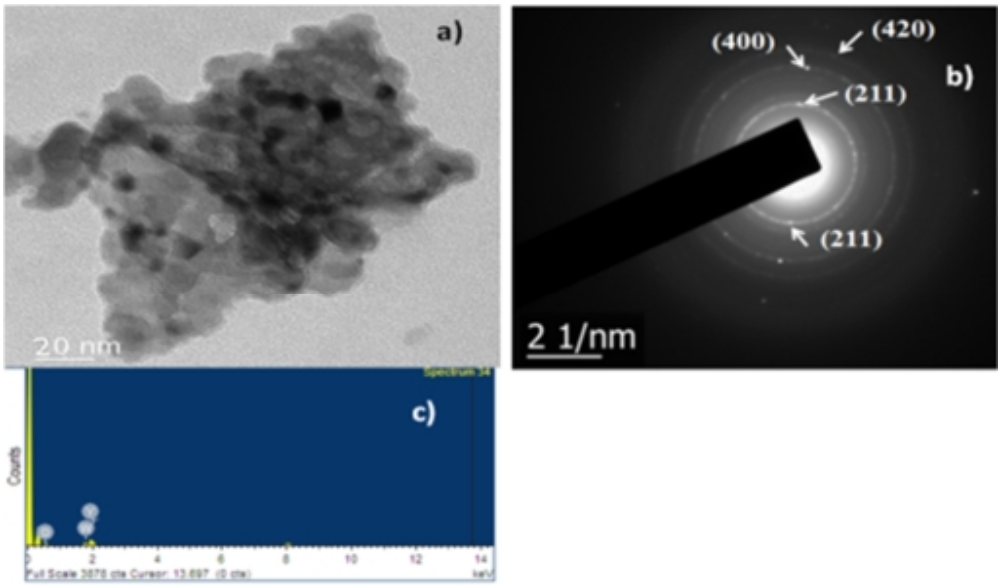

Fig. 7 (a) Bright Field TEM image of 20 h milled $W_{79}Ni_{10}Mo_{10}(Y_2O_3)_1$ alloy b) corresponding SAD pattern c) EDS pattern shows presence of elemental W, Y, O.

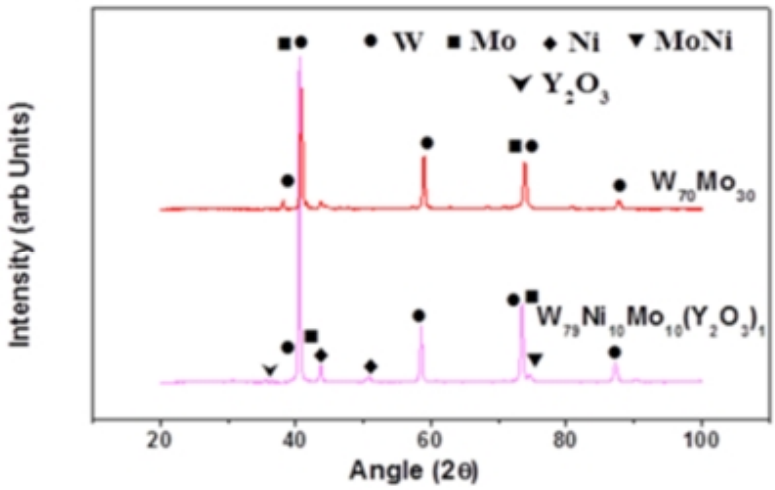

Fig. 8. XRD pattern of alloys $W_{70}Mo_{30}$ and $W_{79}Ni_{10}Mo_{10}(Y_2O_3)_1$ milled for 20 h and sintered at 1500°C for 2 h.

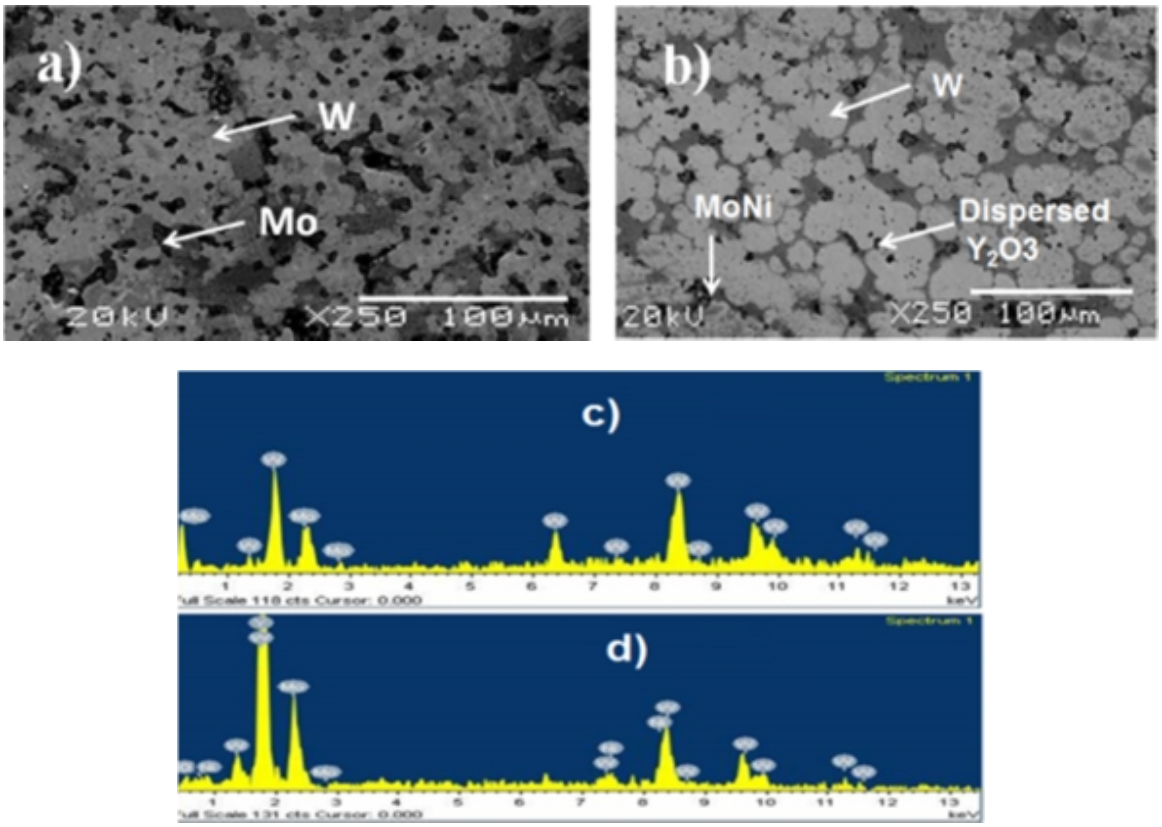

Fig. 9. SEM micrograph of a) $W_{70}Mo_{30}$ and b) $W_{79}Ni_{10}Mo_{10}(Y_2O_3)_1$ alloy milled for 20 h and sintered at 1500°C for 2 h, corresponding EDS pattern of c) $W_{70}Mo_{30}$ d) $W_{79}Ni_{10}Mo_{10}(Y_2O_3)_1$ alloy

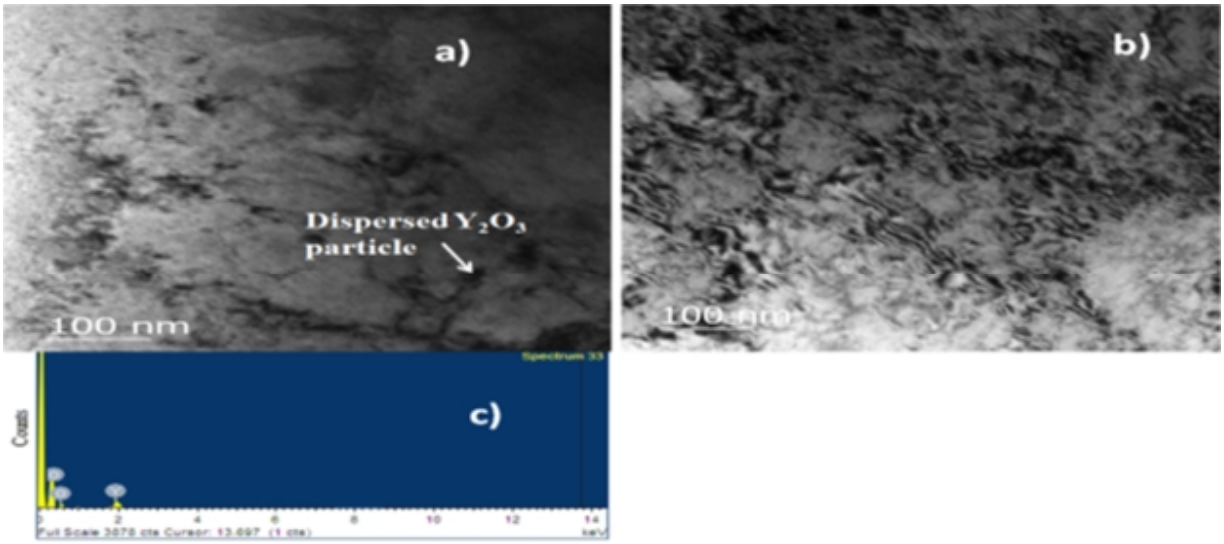

Fig.10. Bright Field HRTEM image of $W_{79}Ni_{10}Mo_{10}(Y_2O_3)_1$ alloy milled for 20h and sintered at 1500°C for 2 h, a) Dispersed Y_2O_3 particles at the grain boundary b) high dislocation density and interaction between dislocation and precipitate particles c) EDS pattern of the dispersed Y_2O_3 particle.

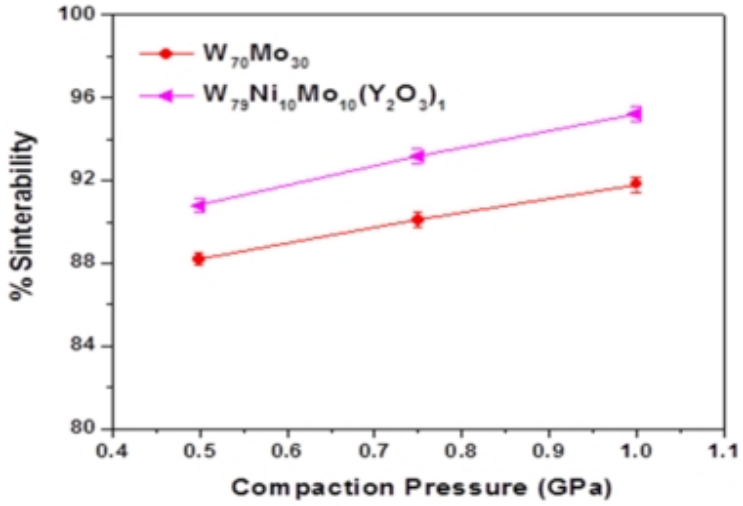

Fig. 11. Variation of sinterability for $W_{70}Mo_{30}$ and $W_{79}Ni_{10}Mo_{10}(Y_2O_3)_1$ alloys milled for 20 h and sintered at 1500°C for 2 h.

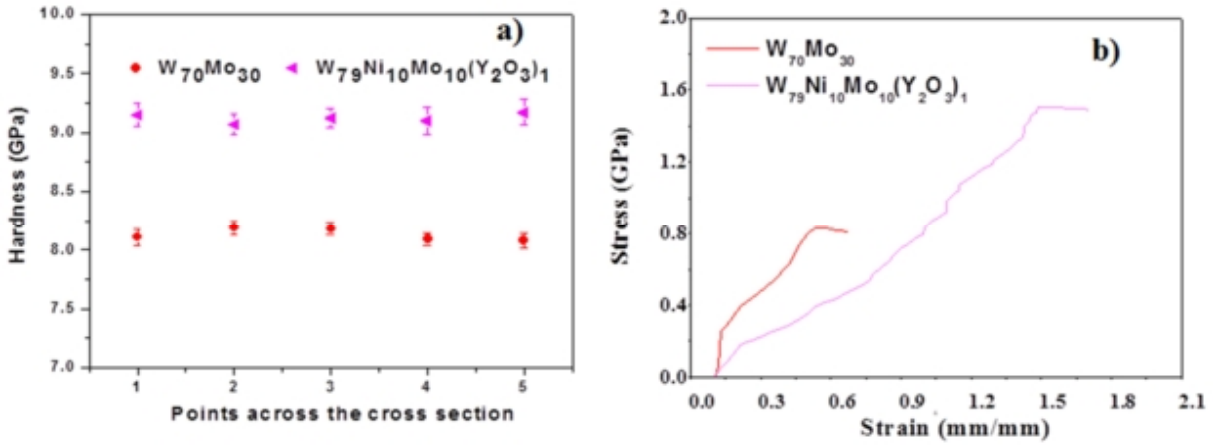

Fig. 12. Variation of a) Hardness b) Compressive Stress-Strain for $W_{70}Mo_{30}$ and $W_{79}Ni_{10}Mo_{10}(Y_2O_3)_1$ alloys milled for 20 h and sintered at 1500℃ for 2 h.

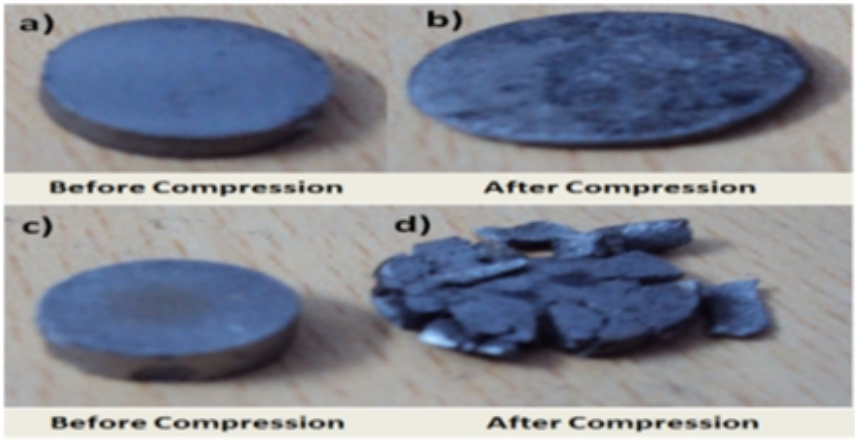

Fig. 13. Geometry of sintered $W_{79}Ni_{10}Mo_{10}(Y_2O_3)_1$ (a, b) and $W_{70}Mo_{30}$ (c, d) before compression and after compression respectively.

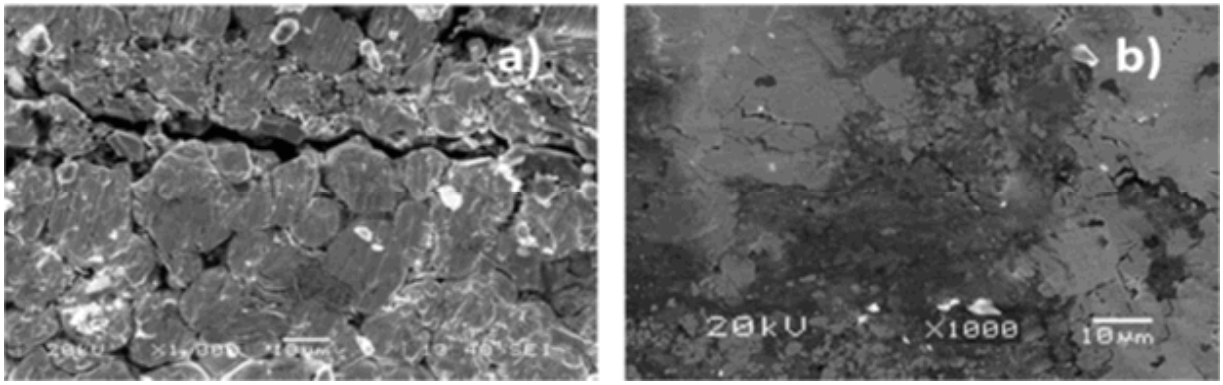

Fig. 14. SEM image of fracture surface of a) $W_{70}Mo_{30}$ b) $W_{79}Ni_{10}Mo_{10}(Y_2O_3)_1$alloy.

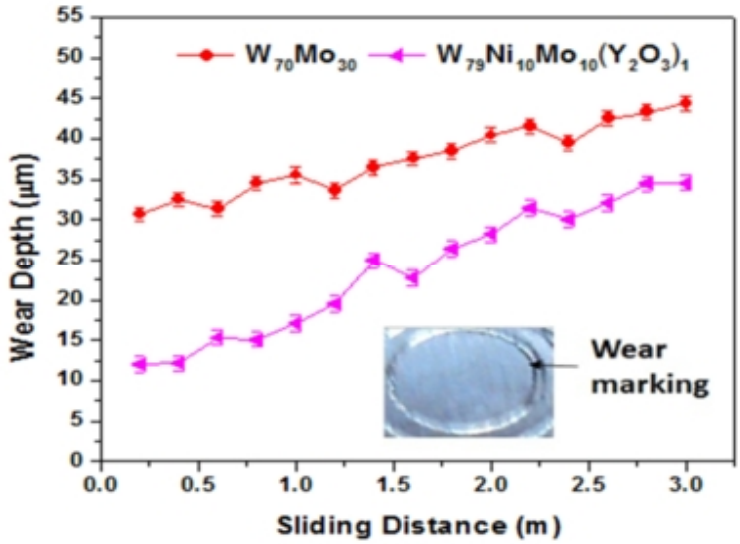

Fig. 15. Variation of Wear depth for $W_{70}Mo_{30}$ and $W_{79}Ni_{10}Mo_{10}(Y_2O_3)_1$ alloys milled for 20h and sintered at 1500°C for 2 h.

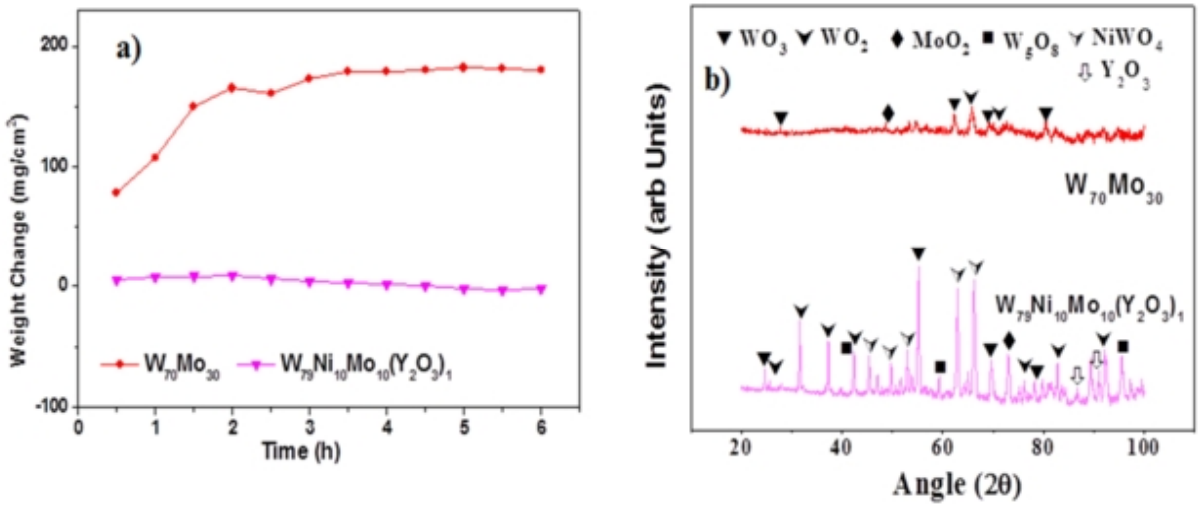

Fig. 16. a) Weight change as a function of exposure time b) Corresponding XRD Pattern for the oxidation of alloys $W_{70}Mo_{30}$ and $W_{79}Ni_{10}Mo_{10}(Y_2O_3)_1$ at 1000°C for 6 h.

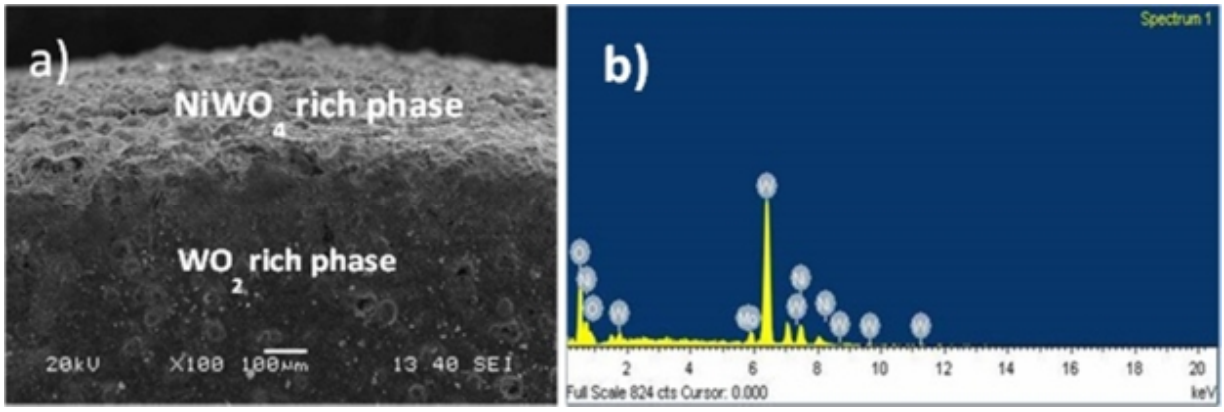

Fig. 17. (a) SEM micrograph of oxidized surface of $W_{79}Ni_{10}Mo_{10}(Y_2O_3)_1$ alloy after exposure at 1000°C for 6 h in air and b) EDS pattern of the oxidized surface displays the presence of W, Ni, Mo, O on the oxide scale.

Conclusions:

Nanostructured W-Mo, and nano-Y_2O_3 dispersed W-Ni-Mo alloy powders are prepared with variation in composition. XRD analysis of all the alloys shows enhanced solid solubility, pointing that Ni, Mo dissolved in W matrix with ball milling for 20h. The nano-Y_2O_3 dispersed W-Ni-Mo alloy shows minimum crystallite size of 29.4 nm and maximum lattice strain and dislocation density of 0.51% and 18.93 ($10^{16}/m^2$) respectively due to high surface energy associated with nano-Y_2O_3. The lattice parameter for both alloys shows an increasing trend at 10 h due to exertion of negative hydrostatic pressure by nano-crystals and decreasing trend at 20 h of milling due to formation of solid solution. Maximum sintered density of 95.2% is achieved with addition of 10 wt. % Ni and 1 wt. % Y_2O_3. The presence of 1.0 wt. % Y_2O_3 increases the hardness, strength to 9.12 GPa and 1.51 GPa respectively as well as wear resistance of the W-Ni-Mo alloy due to presence of MoNi intermetallic phase and dispersion strengthening effect induced by Y_2O_3 particles. The oxidation resistance of 1.0 wt% nano-Y_2O_3 dispersed W-Ni-Mo alloy shows promising results as compared to rest of the alloys in terms of application at elevated temperature. The novelty of the present investigation lies in preliminary encouraging comparative study of room temperature compressive, wear, and high temperature oxidation behavior of ODS and non ODS alloys of W.

Acknowledgements

The research work is funded by TEQIP II, NIT Rourkela. I am grateful to Prof. S.Das, Mr. Tapas Paul, Mr. Sudipta Mandal of IIT Kharagpur for providing me the TEM sample preparation facility and Prof. Rahul Mitra, Mr. Amit Kr. Sarkar, Rahul Mitra of IIT Kharagpur for carrying out the TEM study for both powder and bulk sample.

References

[1] W. F. Smith, Structure and Properties of Engineering Alloys, Second Edition, McGraw-Hill, USA, 1993.

[2] Anshuman Patra, Microscopy and analysis, **26(5)** 2012, 14-19.

[3] R. Malewar, K.S. Kumar, B.S. Murty, B. Sarma, S.K. Pabi, J.Mat.Rev, **22** (2007) 1200-1206

[4] C. Suryanarayana, Prog. Mater. Sci., **46** (2001) 1-184.

[5] C. Suryanarayana, Mechanical Alloying and Milling, Marcel Dekker Inc, New York, 2004, pp. 13.

[6] H. Glieter, Acta. Met., **48** (2001) 1.

[7] G. K. Williamson and W. H. Hall, Acta Mater, **1**(1953) 22.

[8] G. K. Williamson and R. E. Smallman, Philos Mag, **1(1)** (1956) 34–46.

[9] R. E. Smallman, K.H. Westmacott, Philos Mag, **2(17)** (1957) 669–683.

[10] Y. H. Zhao, H. W. Sheng, and K. Lu, Acta Mater, **49** (2001) 365–375.

[11] Michael Robert Middlemas,ProQuest UMI Dissertations Publishing, DAI-B70/0 6 2009, 107-108.

[12] Necati Ozkan & Brian J. Briscoe, J. Eur. Ceram. Soc., **14** (1994) 143-151.

[13] Suresh Telu , A. Patra , M. Sankaranarayana , R. Mitra , S. K. Pabi, Int. Jou of Refract Met and Hard Mater, **36** (2013) 192-194.

[14] M. Nuthalapati, S.K. Karak, J. Dutta Majumdar, A. Basu, Metall. Mater. Trans. A, **45A** (2014) 3748-3754.

[15] S. Sheibani, S. Heshmati-Manesh, A. Ataie, Acta Mater, **58** (2010) 6828–6834.

[16] P. P. Chattopadhayay, P. M.G. Nambissan, S.K. Pabi and I. Manna, Appl. Surf. Sci.182 (2001) 308-312.

[17] G. Dieter: Mechanical Metallurgy: SI Metric Edition, McGraw-Hill Co., Singapore, (1928) 189–93.

[18] P. B. Kemp, R. M. German, Jou. Less. Common Met, **175** (1991) 353-368.

[19] W. J. Quadakkers, J. Phys. IV, **3** (1993) 177-186.